Hybrid Biomechanical Design of Dental Implants: Integrating Solid and Gyroid TPMS Lattice Architectures for Optimized Stress Distribution

Dawit Bogale Alemayehu , Masahiro Todoh , and Song-Jeng Huang *

Posted Date: 9 September 2024

doi: 10.20944/preprints202409.0694.v1

Keywords: finite element method; implantology; biomechanical; additive manufacturing; dental implant; osseointegration; hybrid

Article

Hybrid Biomechanical Design of Dental Implants: Integrating Solid and Gyroid TPMS Lattice Architectures for Optimized Stress Distribution

Dawit Bogale Alemayehu [1], Masahiro Todoh [2] and Song-Jeng Huang [3,*]

[1] Division of Human Mechanical Systems and Design, Graduate School of Engineering, Hokkaido University, Sapporo 060-8628, Japan
[2] Division of Mechanical and Aerospace Engineering, Faculty of Engineering, Hokkaido University, Sapporo 060-8628, Japan
[3] Department of Mechanical Engineering, National Taiwan University of Science and Technology, Taipei 10607, Taiwan
* Correspondence: sgjghuang@mail.ntust.edu.tw

Abstract: Dental implantology has evolved greatly as a result of the application of biomechanical engineering concepts, notably the utilization of additive manufacturing technologies that recreate the intricate architecture of real bone. This technique intends to improve functional compatibility with bone tissue while also addressing continuing problems of stress distribution inside dental implants. The research examines two types of dental implants: fully gyroid latticed and hybrid gyroid latticed with a solid neck, comprising three different cell sizes—FI-111, FI-222, FI-333, and their hybrid equivalents HI-111, HI-222, and HI-333. Traditional solid implants often cause stress shielding, which reduces long-term osseointegration and implant durability. Developed using nTopology for lattice configuration and meshing, this design undergoes a comprehensive stress analysis using finite element analysis (FEA). The study seeks to determine the most efficient implant design by maximizing stress distribution and mechanical stiffness. Analyses suggest that hybrid latticed implants, notably the HI-222 type, possess superior mechanical characteristics. These implants successfully balance stiffness and flexibility, reducing stress concentrations and improving stress distribution throughout the implant structure. This balance is critical for decreasing micromotions at the bone-implant interface, boosting osseointegration, and, ultimately, increasing implant longevity and success rates in clinical settings. The paper describes a substantial redesign of dental implants by combining biomechanical engineering and modern additive manufacturing. The novel proposed hybrid structure not only addresses typical challenges such as stress shielding, but it also establishes new standards in implantology, potentially leading to better clinical results and patient quality of life. This complete approach emphasizes the ability of personalized implant designs to fulfill individual clinical demands, indicating a significant improvement in dental treatment technology.

Keywords: finite element method; implantology; biomechanical; additive manufacturing; dental implant; osseointegration; hybrid

1. Introduction

The lattice structure, a subset of the triply periodic minimum surfaces (TPMS) family, has a highly interwoven and sophisticated architecture, with the gyroid TPMS lattice standing out as a particularly notable subtype [1–3]. Many industries, particularly dental applications and the broader field of tissue engineering, praise this structure for its immense potential [4]. Its intricate and precision-driven design is ideal for incorporation into dental implants, where rigorous standards are required [5,6]. The gyroid lattice enables the precise adjustment of sophisticated geometric

 doi:10.20944/preprints202409.0694.v1

arrangements to meet specific medical requirements. This potential is the result of taking advantage of cutting-edge 3-D printing technology [7,8].

The porous structure of the gyroid lattice makes it ideal for tissue engineering applications[9–11]. These structures' particular porosity promotes vascularization and cell proliferation, both of which are required for implants to successfully integrate with surrounding biological tissues [12–14]. Throughout the 3-D printing process, precise regulation of this porosity enables excellent bone ingrowth and osseointegration, crucial for the long-term success of dental implants [15–17]. Furthermore, the intrinsic complexity of lattice geometry, rather than being a disadvantage, is a tremendous benefit in the age of additive manufacturing [10,18,19].

The higher porosity of the gyroid TPMS lattice improves both structural integrity and osseointegration where the implant meets the bone [20–22]. This feature is crucial for the long-term success of dental implants by promoting better bone in growth and stability [23,24]. These structures' versatility in responding to many forms of advanced manufacturing, particularly additive manufacturing, emphasizes their usefulness even more. Since the introduction of additive manufacturing technology, the capacity to produce intricate and complicated structures such as gyroid TPMS lattices has transformed dental implant design [10,25]. Among the many current manufacturing processes, laser powder bed fusion (L-PBF) and other metal 3D printing techniques stand out. L-PBF, in particular, offers a highly effective solution for creating implants with detailed internal architectures [26]. Its capacity to deposit material precisely layer by layer makes it appropriate for both tissue engineering scaffolds and complicated dental implants [27–29]. Commercially, pure titanium and its alloys are the preferred materials for these applications because they are known for their superior mechanical qualities and biocompatibility, making them perfect for medical use [30–34].

Usually, exact equations regulate the design and characteristics of lattice structures, which are complex mathematical creations [35–37]. These elaborate designs are not just theoretical but also have practical applications in a variety of sectors, owing to the employment of advanced computational tools. A recent study used MATLAB, a robust numerical computing environment, to develop code that explicitly specifies and manipulates the geometry of lattice structures [38], enabling a high degree of customization and accuracy. Furthermore, intuitive design and engineering software tools, such as ANSYS SpaceClaim, provide user-friendly interfaces for building and updating 3D models, allowing designers to explore complicated lattice geometries more easily [39]. CAD software, such as PTC Creo Parametric, provides robust tools for detailed design and engineering, which is critical for integrating specific mechanical requirements of lattice structures into functional products [40,41], whereas nTopology optimization software stands out for its ability to fine-tune designs for performance criteria, making it invaluable in optimizing architectural efficiency [42]. The gyroid lattice implant demonstrates how these various software applications may work together to create a very practical and unique design [10,11,43]. We used these sophisticated techniques to create the basic CAD model for this implant, showcasing the flexibility and adaptability of lattice design across diverse applications [44–47]. Engineers and designers can use sophisticated software solutions to push the boundaries of what is possible in lattice fabrication, resulting in breakthroughs in fields ranging from aerospace to biomedical engineering, emphasizing the collaborative role of various advanced software in refining and realizing these designs [46,48–50].

In research, the Finite Element Method (FEM) is a well-known numerical technique that not only reduces material waste but also saves money and time, improving overall efficiency in engineering projects [51–57]. Most FEM research has primarily focused on using quasi-static loading analysis to effectively simulate the compression behavior of lattice structures, which is critical for evaluating their structural integrity under varying load situations [53]. However, despite its widespread use, only a few studies have investigated the possibilities of dynamic explicit analysis [58,59]. This approach has demonstrated high dependability in confirming experimental results by precisely mimicking real-world dynamic impacts and stress conditions that lattice structures may experience [60–63]. The effectiveness of dynamic explicit analysis in generating informative data and exposing unique response characteristics under dynamic loading situations offers a potential field of study that

 doi:10.20944/preprints202409.0694.v1

is mostly unexplored [52]. Given this context, the current work aims to delve deeper into this understudied topic.

The main goal of this study is to use explicit dynamic finite element analysis to fully understand how initially fully latticed dental implants behave mechanically when they are under dynamic load. Based on these analytical findings, the project intends to systematically create an optimum dental implant with a novel hybrid design. This design combines a solid neck with a lattice construction for the rest of the implant, with a focus on improving biomechanical compatibility and structural stability. The hybrid structure aims to minimize stress accumulation in crucial areas of the implant, particularly the neck and first thread, which have the highest risk of failure. Using the Finite Element Method (FEM), this study thoroughly assesses stresses and strains inside the implant structure, providing a solid basis for improving the suggested design. This extensive evaluation not only improves the ability to comprehend stress distribution patterns, but it also allows for implant optimization to better resist physiological loading conditions. We expect the hybrid latticed structure to outperform the completely latticed design in terms of optimizing mechanical characteristics and controlling micromotions under cyclic masticatory stress. Finally, the goal of this work is to transform these thorough analytical insights into real advantages in implant design, perhaps creating new standards in dentistry and providing major benefits in patient care.

2. Materials and Methods

2.1. Assembly CAD Model and 2D Drawing

Creo Parametric version 8.0 software precisely designed the dental implant system's primary components, including cancellous and cortical bone structures. As seen in Figure 1, the software assisted in the creation of both two-dimensional drawings and three-dimensional models, ensuring that all dimensions were appropriately displayed. The primary focus of this design effort is the implant itself, which will incorporate a Gyroid lattice structure in various configurations, including both fully and hybrid latticed dental implant designs. This method not only enhances the implant's visibility in its functional environment, but also enables precise design modifications specifically tailored to integrate the Gyroid lattice structure efficiently.

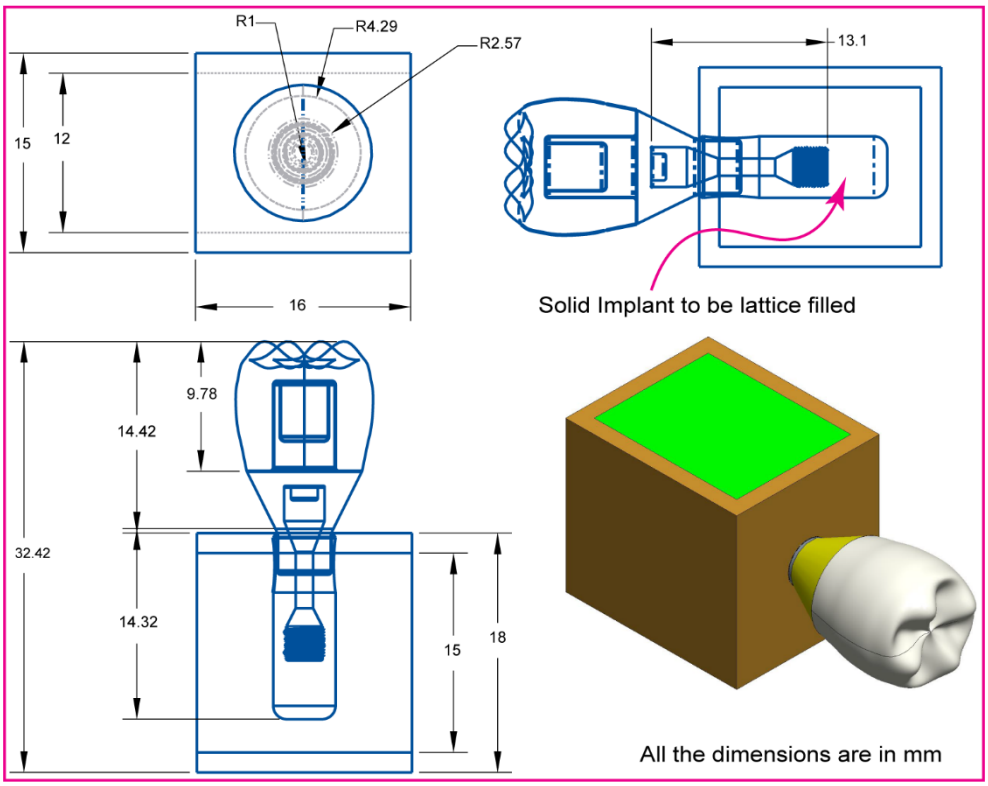

 doi:10.20944/preprints202409.0694.v1

Figure 1. Assembled implant system 3D and 2D drawings.

2.2. Dental Implant Lattice Design

Figure 2 shows a dental implant filled with a Gyroid lattice structure in two different layouts. These layouts include fully and hybridly latticed dental implant designs that use three different cell sizes, which are 111, 222, and 333. The three-dimensional (3D) model employed in this work was based on a rectangular slice of cortical and trabecular bone extracted from a human jaw. We methodically created the original implant design using PTC Creo Parametric, a powerful Computer-Aided Design (CAD) application. We accurately established the specific dimensions of each model, which included a length of 14.32 mm, a diameter of 4.1 mm, and a wall thickness of 0.8 mm. This accuracy in design parameters guarantees that the implants are ideally structured to fulfill particular biomechanical criteria and allows for the examination of structural variations dependent on cell size within lattice designs.

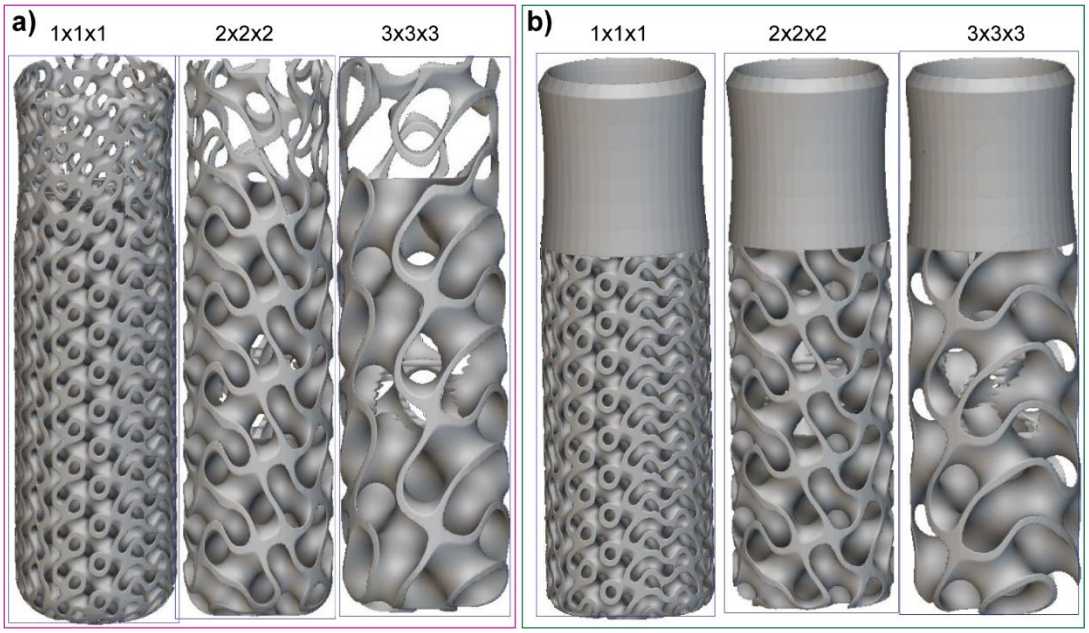

Figure 2. Dental Implant Models with a) Fully, and b) Hybrid Gyroid Lattice Configurations.

2.3. Dental Implant FE-Meshing and Mechanical Properties

Figure 3 illustrates the process of saving the dental implant configurations within the system components as SAT file extensions. We then export these files to nTopology for the creation of finite element meshes. Both the fully latticed and hybrid latticed dental implants use three distinct cell sizes: 111, 222, and 333. We mesh each model using 0.1 mm finite element (FE) sizes and 1.0 mm edge length. 0.1 mm elements mesh the retaining screw and solid neck in the hybrid lattice. The compact bone and spongy porous bone, which are crucial for implant stability, are finer meshed around the implant hole, improving the reliability of stress evaluation in these key locations. On the other hand, we mesh the remaining areas with a coarser element size of 0.3 mm to effectively manage computational resources while maintaining model fidelity. This method of precise meshing ensures the appropriate design of every dental implant system component for structural study, enabling a deeper exploration of the biomechanical characteristics present in both fully and hybrid latticed systems. The mesh statistics for the dental implant, its components, and assembly models are presented in Table 2. This method intends to create a biomimetic scaffold that not only closely resembles the architecture of natural bone, but also maximizes the implant's biomechanical performance by incorporating strategic design changes. And the physical properties of the materials for the dental implant, its components, and bones are listed in Table 1 [52–54].

 doi:10.20944/preprints202409.0694.v1

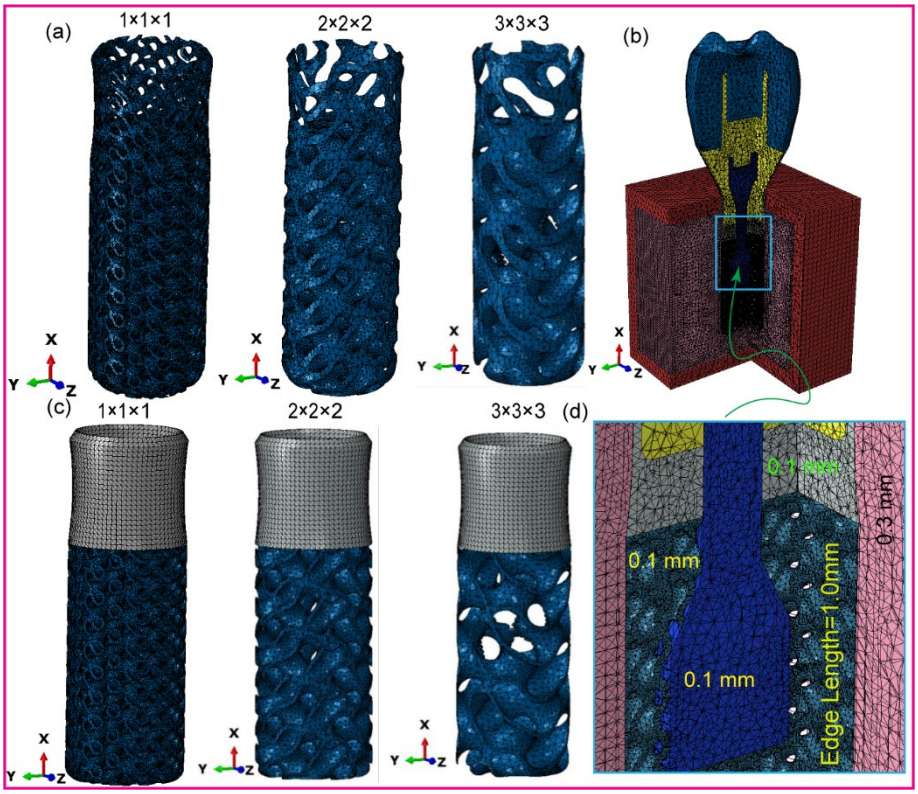

Figure 3. Fe mesh for (a), Fully latticed implant, (b) assembled dental implant, (c) Hybrid latticed implant, and (d) zoomed FE mesh details indicated by rectangle.

2.4. Dynamic Mastication Loading and Boundary conditions

Figures 4a and 4b show the constructed implant system under dynamic load, using one of the two latticed implant designs investigated in this work. Dynamic explicit analysis was used to mimic real-world events that might occur during the implant's clinical usage. This picture (Figure 4a) shows the implant when it is loaded at an angle of 78.58 degrees, with forces acting in the mesiodistal, axial, and buccolingual directions. We subjected the occlusal crown surface to stresses from three different directions—mesiodistal, buccal-lingual, and apical—to evaluate the biomechanical response of the dental implant under multi-axial dynamic oblique loading. We strategically delivered force magnitudes of 23.4 N, 17.1 N, and 114.6 N, converging at an ill-defined reference point 3 mm from the occlusal surface using a multi-point constraint (MPC) technique. We created this arrangement to simulate the complex pressures experienced during clinical mastication, resulting in an equivalent force of 118.2 N, inclined at 75.8 degrees relative to the occlusal plane [52,54]. We reduced the explicit dynamic loading to a slower rate to replicate the cyclic stress of mastication, typically detected at 2 Hz over a 0.5-second interval. Furthermore, carefully created boundary conditions mimicked real-world restrictions at the implant-mandible interface. A six-degree-of-freedom (DoF) Encastre boundary condition held the implant securely in all three spatial dimensions (X, Y, and Z). This made it possible to replicate the stress distribution exactly in many directions. With this thorough setup, exact measurements of compressive and tensile stresses inside the implant system could be made using finite element analysis with ABAQUS 2021. This made the study more reliable.

Preprints.org (www.preprints.org) | NOT PEER-REVIEWED | Posted: 9 September 2024 doi:10.20944/preprints202409.0694.v1

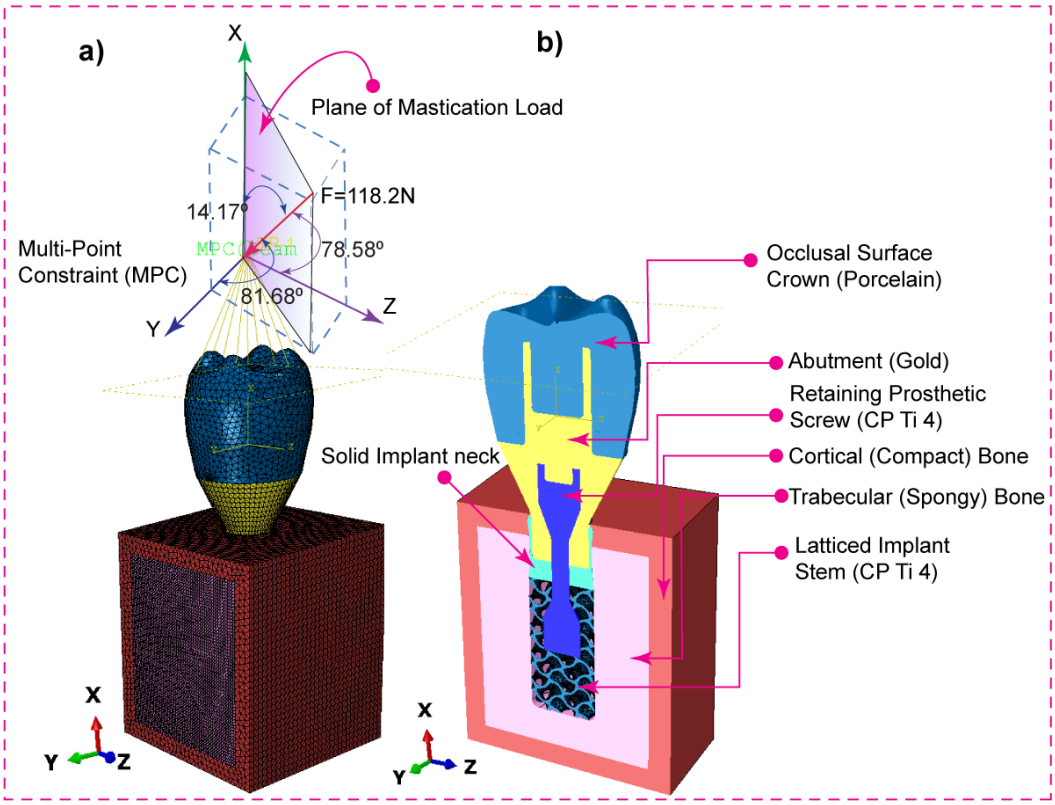

Figure 4. Dental implant system, (a) Dynamic mastication loading for 0.5 sec with 2 Hz in a single cycle, and (b) its components.

Table 1. Mechanical properties off materials for finite element analysis [52–54].

Materials	Young's Modulus E (MPa)		Poisson's Ratio ν		Density (g/cm3)	Strength (MPa)
Cortical bone	E_x	12,600	ν_{xy}	0.3	1.79	190
	E_y	12,600	ν_{yz}	0.253		
	E_z	19,400	ν_{xz}	0.253		
			ν_{yx}	0.3		
			ν_{zy}	0.39		
			ν_{zx}	0.39		
Cancellous bone	E_x	1148	ν_{xy}	0.055	0.45	10
	E_y	210	ν_{yz}	0.01		
	E_z	1148	ν_{xz}	0.322		
			ν_{yx}	0.01		
			ν_{zy}	0.055		
			ν_{zx}	0.322		
Gold abutment *	136,000		0.37		17.5	765
Porcelain	68,900		0.28		2.44	145
Titanium grade 4 *	110,000		0.34		4.5	550

Table 2. FE mesh statistics of fully and hybrid latticed dental implants, implant components, and their assembly models.

	Crown	Abutment	Screw	Implant	Cortical Bone	Trabecular Bone	Total

 doi:10.20944/preprints202409.0694.v1

Implant models	No. Element	No. Node	No. Element	No. Node	No. Element	No. Node	No. Element	No. Node	No. Element	No. Node	No. Element	No. Node	No. Element	No. Node
FI-111	107,954	20,670	85,243	17,463	627,098	121,624	407,478	134,806	75,894	16,979	76,821	14,782	1,290,128	309,416
FI-222	107,954	20,670	85,243	17,463	536,738	104,716	72,654	25,465	75,894	16,979	76,821	14,782	955,304	200,075
FI-333	107,954	20,670	85,243	17,463	536,738	104,716	37,294	12,640	75,894	16,979	76,821	14,782	919,944	187,250
HI-111	32,352	6,658	23,665	5,331	627,098	121,624	408,753	126,828	75,775	16,948	755,638	136,485	1,372,798	309,700
HI-222	32,352	6,658	23,665	5,331	47,087	10,674	64,362	21,636	75,775	16,948	755,638	136,485	1,028,407	204,508
HI-333	32,352	6,658	23,665	5,331	47,087	10,674	25,634	9,193	75,775	16,948	755,638	136,485	989,679	192,065

FI-111=Fully latticed implant with 111 cell size, **HI-111**=Hybrid latticed implant with 111 cell size.

3. Results

3.1. Cyclic Mastication Loading

Figure 7 shows how an oblique dynamic load of 118.2 N is applied to the occlusal surface of a dental crown in the buccal-lingual, axial, and mesiodistal directions. This loading replicates a 2 Hz mastication cycle, which accurately reproduces the dynamic stress patterns over a 0.5-second period. The figure depicts increasing load variation throughout the mesiodistal, buccal-lingual, and apical orientations, revealing a smooth shift in load amplitude. The use of multi-point constraints (MPC) with a reference point as the master control considerably improved the accuracy of masticatory force replication, reflecting the complex dynamics found in clinical situations. This technique verified that the load distribution closely matched the parameters established in earlier research [32], hence proving the validity of the simulated masticatory forces on both completely and hybrid latticed dental implants. The cell sizes of the fully latticed designs were FI-111, FI-222, and FI-333, while the hybrid latticed designs were HI-111, HI-222, and HI-333. The results of this explicit dynamic loading and the related boundary conditions closely matched previous findings, demonstrating the simulation's resilience in representing real-world biomechanical phenomena.

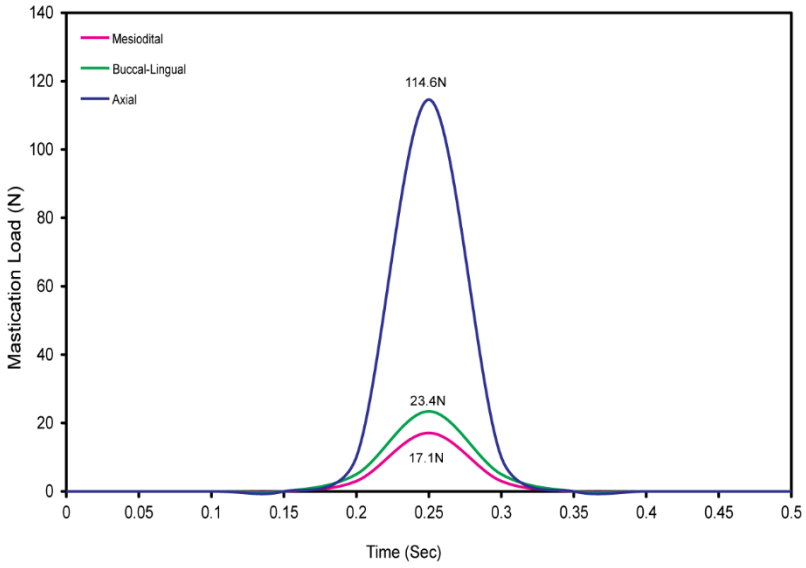

Figure 5. Oblique dynamic loading distribution at 118.2 N in buccal-lingual, axial, and mesiodistal directions over a 0.5-second mastication cycle.

 doi:10.20944/preprints202409.0694.v1

3.2. Maximum von Mises Stress in Dental Implant Assembly

3.2.1. Fully Latticed Dental Implant

Figure 6 presents the highest von Mises stresses that were found in three totally gyroid latticed dental implants with different-sized cells. The smallest cell-size implant, FI-111 (1x1x1), has the greatest stress, measured at 777.65 MPa. This degree of stress indicates a more concentrated load-bearing capability, perhaps because of the narrower lattice structure, which may give less dispersion room for stress. In comparison, the FI-222 implant, with a cell size of 2x2x2, showed a decrease in von Mises stress of 450.31 MPa. This suggests increased stress distribution capabilities, most likely due to the larger cell size, which allows for more efficient mechanical force dispersion over the implant structure. The biggest cell size studied, FI-333 (3x3x3), had the lowest von Mises stress of 388.05 MPa. This further decline implies that the implant's capacity to disperse mechanical stress increases with cell growth, leading to reduced total stress levels.

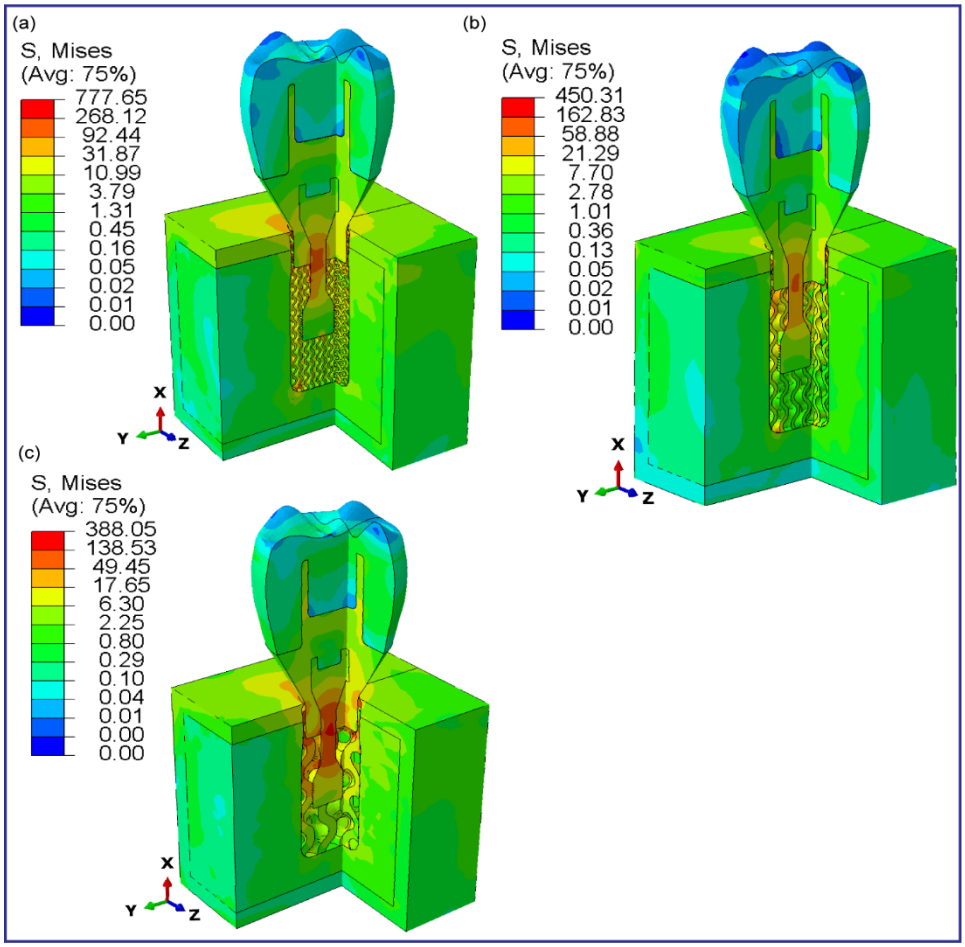

Figure 6. FEA Stress Contour Plots for von Mises stress distributions in assembled and cross-sectioned views of three fully gyroid latticed dental implants with varying cell sizes: a) FI-111, b) FI-222, and c) FI-333.

3.2.2. Hybrid Latticed Dental Implant

Figure 7 displays how the stresses behave under simulated biting forces for the highest von Mises stresses in three hybrid gyroid latticed dental implants, whose cell sizes were changed. The HI-111 implant, with a 1x1x1 cell size design, has a maximum stress of 372.8 MPa. Because HI-222 has a slightly greater stress level (420.53 MPa) due to its larger cell size of 2x2x2. In contrast, the largest cell-size implant, HI-333 (3x3x3), had a lower stress value of 355.22 MPa. These findings indicate that

 doi:10.20944/preprints202409.0694.v1

among hybrid latticed designs, the implant with a medium cell size suffered the most stress, while both smaller and larger cell topologies resulted in lower stress levels.

In contrast, in the case of completely latticed implants, as cell size rose from FI-111 to FI-333, von Mises stress decreased consistently, demonstrating that larger cell sizes result in better stress distribution. The hybrid latticed implants, on the other hand, showed a non-linear pattern, with the largest stress recorded in the medium cell size (HI-222). This was different from the trend seen in the fully latticed implants. This variation emphasizes the complicated relationship between lattice architecture and stress distribution in dental implants.

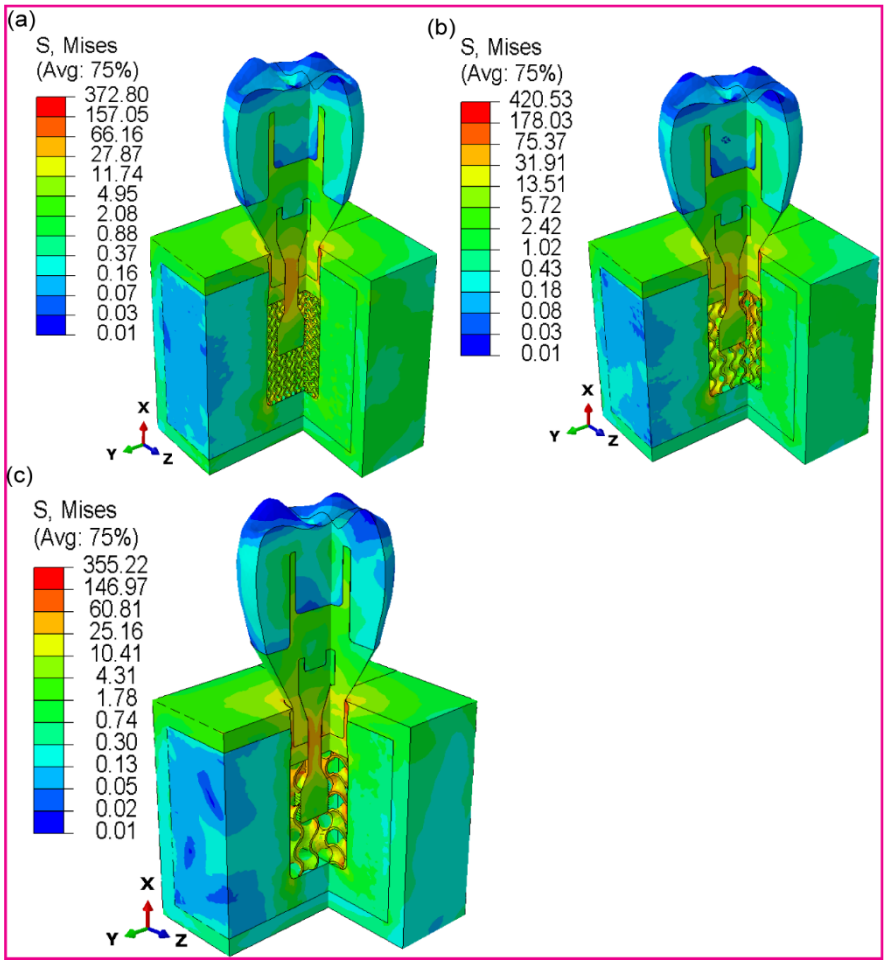

Figure 7. FEA Stress Contour Plots for the von Mises stress distributions in assembled and cross-sectioned views of three hybrid gyroid latticed dental implants, each with different cell sizes: a) HI-111, b) HI-222, and c) HI-333.

3.2.3. Fully and Hybrid Latticed Dental Implant and Retaining Screw

Figure 8 shows a comparison of the maximum von Mises stresses for completely gyroid latticed and hybrid gyroid latticed dental implants, as well as their corresponding retention screws, across various cell sizes. Fully latticed implants show a clear pattern in which von Mises stress reduces with increasing cell size. The FI-111 implant, with the lowest cell size of 1x1x1, had the maximum stress at 410.1 MPa. The high stress level indicates that smaller lattice cells may concentrate stress more than larger ones. The FI-222 and FI-333 implants, with cell sizes of 2x2x2 and 3x3x3, respectively, demonstrated reduced stress values of 322.1 MPa and 300.95 MPa. As the cell size rises, the stress distribution over the implant structure improves, possibly increasing the implant's endurance and performance.

The retention screws associated with these implants showed similar stress patterns (refer to Figure 9), with the FI-111 screw having the maximum stress at 450.31 MPa and subsequently

 doi:10.20944/preprints202409.0694.v1

decreasing in the FI-222 and FI-333 screws to 322.1 MPa and 320.31 MPa, respectively. This pattern highlights the impact of cell size on the mechanical stability of not just implants but also essential components like screws, which play an important part in the whole implant system.

In contrast, the hybrid latticed implants showed a more variable pattern of stress distribution. The HI-111, with a cell size of 1x1x1, had a stress of 344.06 MPa, which was

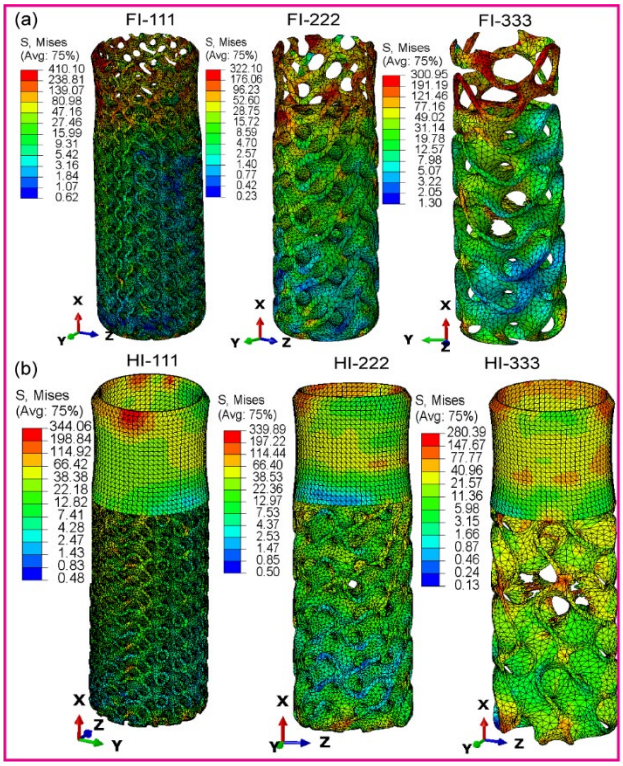

Figure 8. Maximum von Mises Stress distributions for fully and hybrid gyroid latticed dental implants across various cell sizes: (a) FI-111, FI-222, FI-333, dental implants for fully latticed implants, (b) HI-111, HI-222, HI-333, Dental implants for hybrid latticed implants.

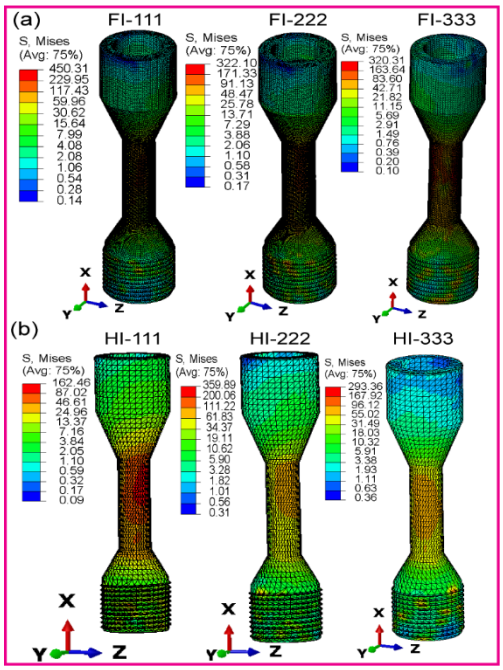

 doi:10.20944/preprints202409.0694.v1

Figure 9. Maximum von Mises Stress distributions for fully and hybrid gyroid latticed dental implants for retaining screws across various cell sizes: (a) FI-111, FI-222, FI-333, retaining screws for fully latticed implants, (b) HI-111, HI-222, HI-333, retaining screws for hybrid latticed implants.

lower than its completely latticed sibling but still considerable. The HI-222 and HI-333 implants reported values of 339.89 MPa and 280.39 MPa, respectively, demonstrating a less consistent drop in stress with increasing cell size than the completely latticed models. The stresses in the retaining screws for these hybrid models also varied, with the HI-111 screw having a significantly lower stress at 133.03 MPa, implying that the hybrid design may affect stress distribution differently, possibly due to variations in structural integrity or load-bearing pathways within the implant.

3.2.4. Fully and Hybrid Latticed in Cortical and Cancellous Bone

The figures 10 show in detail the highest von Mises stresses in the cortical and cancellous bones that are connected to fully hybrid latticed dental implants at various cell sizes. The von Mises stress results for the fully latticed implants (FI-111, FI-222, and FI-333) show considerable differences depending on cell size and bone type. FI-333 had the maximum stress in the cortical bone at 65.46 MPa, indicating a significant concentration of stress, especially in the implant-bone interface around the neck, where the implant and bone are in close contact. This region is crucial because it absorbs the majority of mechanical stresses during mastication. In contrast, FI-222 exhibits the lowest stress in cortical bone at 34.86 MPa, suggesting a more advantageous stress distribution that may improve implant lifetime and lower the risk of bone resorption.

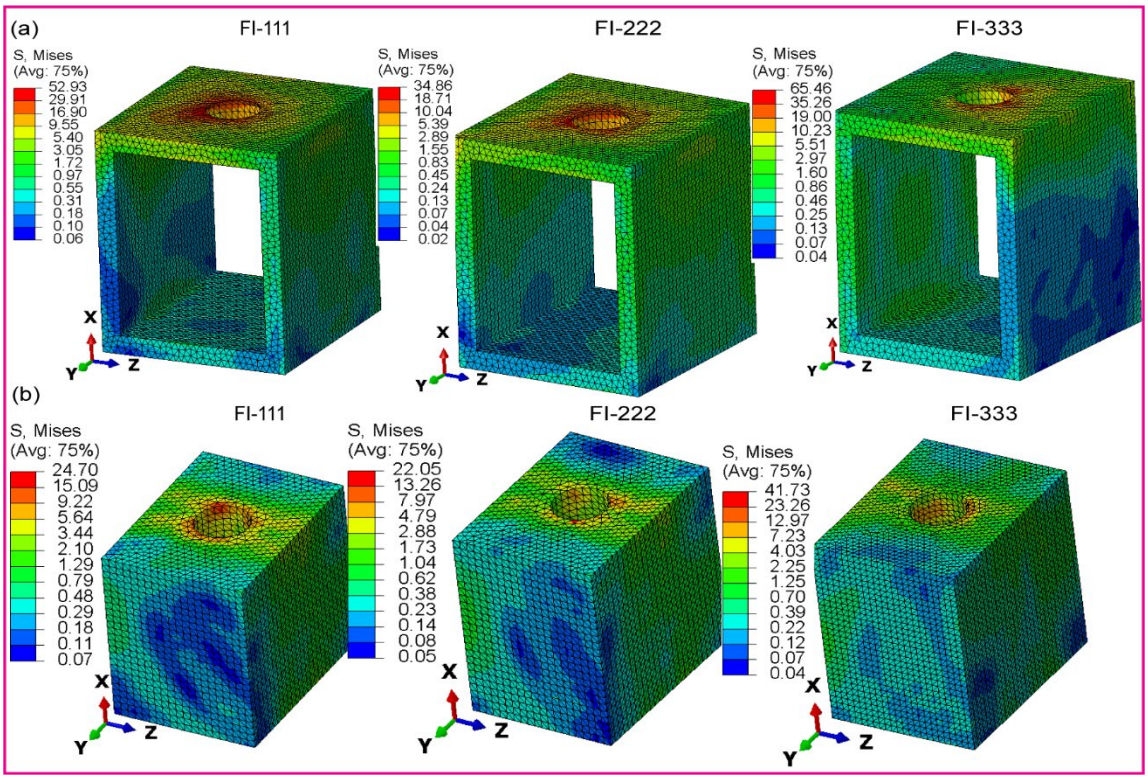

Figure 10. Maximum von Mises Stress distributions for fully gyroid latticed dental implants across various cell sizes (FI-111, FI-222, FI-333) for: (a) cortical bone, and (b) cancellous bone.

In Figure 10b, the FI-333 again records increased stress at 41.73 MPa for the cancellous bone. This is consistent with studies in cortical bone and highlights a pattern in which larger cell sizes could aggravate stress concentrations, particularly around the implant neck and hole. Meanwhile, FI-111 and FI-222 exhibit lower stresses (24.7 MPa and 22.05 MPa, respectively), suggesting that smaller cell sizes may reduce stress peaks in less dense bone formations.

 doi:10.20944/preprints202409.0694.v1

The stress levels in the cortical and cancellous bones for hybrid gyroid latticed dental implants with a solid neck (HI-111, HI-222, and HI-333) are shown in Figure 11. The HI-333 model, in particular, has the maximum stress level inside the cancellous bone (44.23 MPa). The implant hole, a crucial area where the implant closely contacts the bone, concentrates this peak stress. Such a high stress concentration is important because it shows places where the implant's structure and overall therapeutic performance could be damaged. This suggests that the HI-333 cell size and lattice design may not be as good at distributing stress.

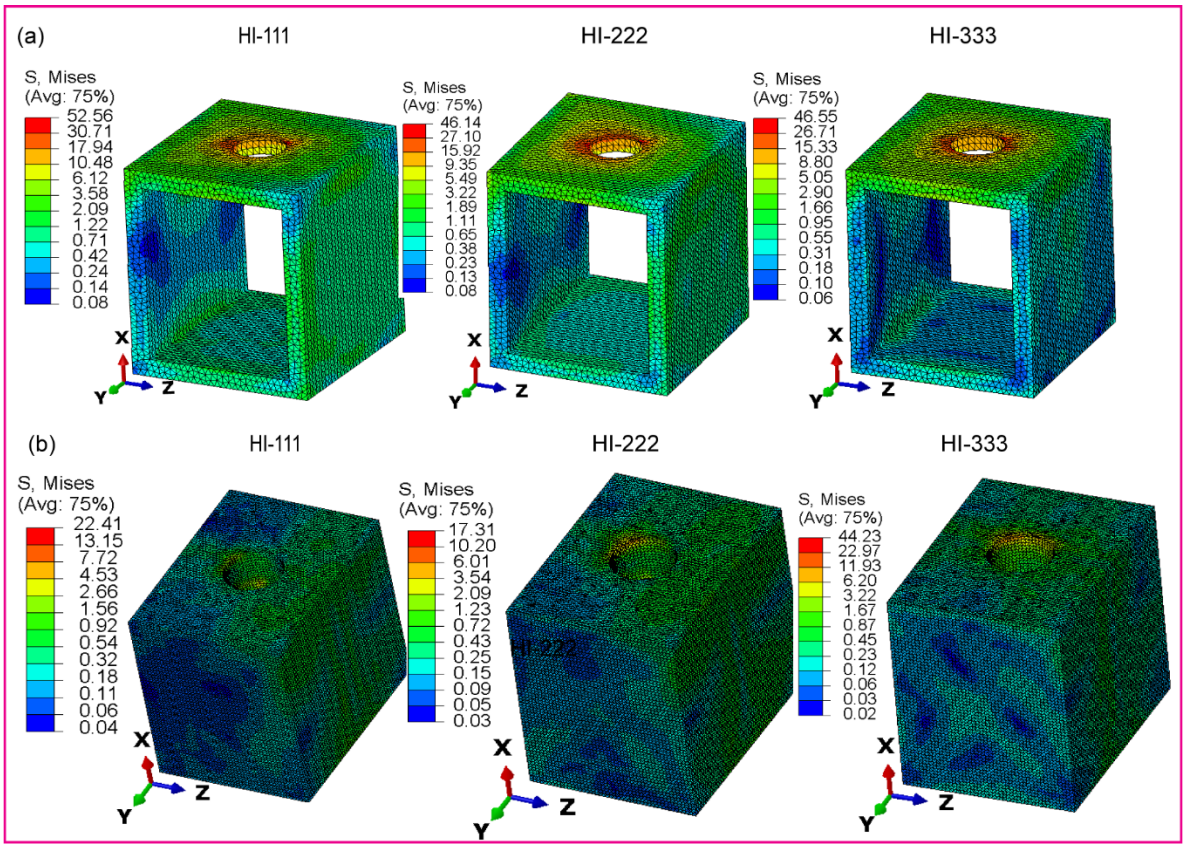

Figure 11. Maximum von Mises Stress distributions for hybrid gyroid latticed dental implants across various cell sizes (HI-111, HI-222, HI-333) for: (a) cortical bone, and (b) cancellous bone.

In contrast, the HI-222 implant exhibits substantially lower stress levels, with 46.14 MPa in cortical bone and a remarkably low 17.31 MPa in cancellous bone. These results indicate that the HI-222's lattice architecture and cell size are very efficient in distributing stresses throughout the implant structure. This optimum stress mitigation not only increases the implant's longevity but also reduces the likelihood of bone resorption and implant failure, suggesting better biomechanical performance compared to its contenders.

3.2.5. Fully and Hybrid Latticed in Crown and Abutment

The highest von Mises stresses can be seen in Figures 12 and 13, which show the crown and abutment parts of fully and hybrid latticed dental implants with three different cell sizes. The crown components of fully latticed implants (Figure 12) had relatively low stress values, with FI-111 reporting 4.29 MPa, FI-222 at 2.72 MPa, and FI-333 at 3.46 MPa. On the contrary, the abutment components in the same group experience notably higher stresses: FI-111 at 219.23 MPa, FI-222 at 777.65 MPa, and FI-333 at 283.07 MPa.

Conversely, the hybrid latticed implants (Figure 13) demonstrate comparatively higher stress levels in the crown compared to their fully latticed counterparts, with HI-111 at 6.95 MPa, HI-222 at 6.57 MPa, and HI-333 at the lowest at 2.31 MPa. The abutment stresses in these hybrid models are

Preprints.org (www.preprints.org) | NOT PEER-REVIEWED | Posted: 9 September 2024 doi:10.20944/preprints202409.0694.v1

much lower, resulting in a more balanced stress distribution: HI-111 22.41 MPa, HI-222 17.31 MPa, and HI-333 44.23 MPa.

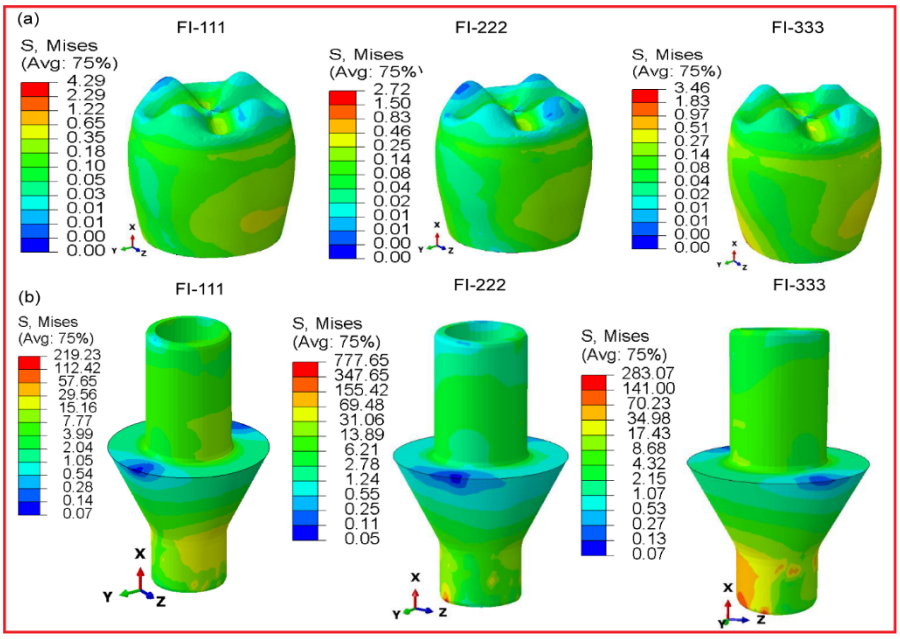

Figure 12. Maximum von Mises Stress distributions for fully gyroid latticed dental implants across various cell sizes (FI-111, FI-222, FI-333) for: (a) crown, and (b) abutment.

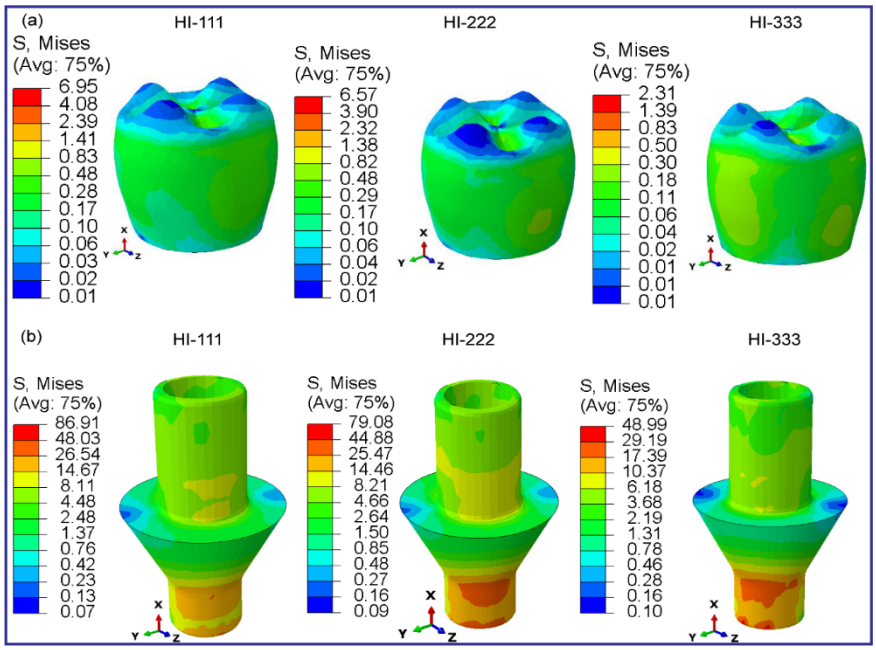

Figure 13. Maximum von Mises Stress distributions for hybrid gyroid latticed dental implants across various cell sizes (HI-111, HI-222, HI-333) for: (a) crown, and (b) abutment.

When compared to completely latticed designs, hybrid latticed implants show a more uniform distribution of stresses between the crown and abutment, as well as lower stress levels in the abutment. The hybrid arrangements, in particular, provide much lower stress in the abutment portion as compared to their completely latticed counterparts, suggesting possibly greater mechanical performance under clinical situations. Furthermore, within each configuration, the crown consistently exhibits lower stresses than the abutment, indicating a significant difference in stress management between these two key components of dental implants.

 doi:10.20944/preprints202409.0694.v1

3.2.6. Micromotions in Assembled Dental Implant for Fully and Hybrid Latticed

Figure 14 shows the movement of fully latticed dental implant setups with different cell sizes (FI-111, FI-222, and FI-333) during a single 0.5-second cycle of mastication oblique loading. At first, displacement in all three designs was zero, indicating strong initial stability under load. However, after roughly 0.215 seconds, displacement shifts negative, reaching -17.5 micrometers for FI-111 and -13 micrometers for FI-333. This negative displacement indicates a slight initial countermovement within the bone-implant interface, possibly due to early load absorption.

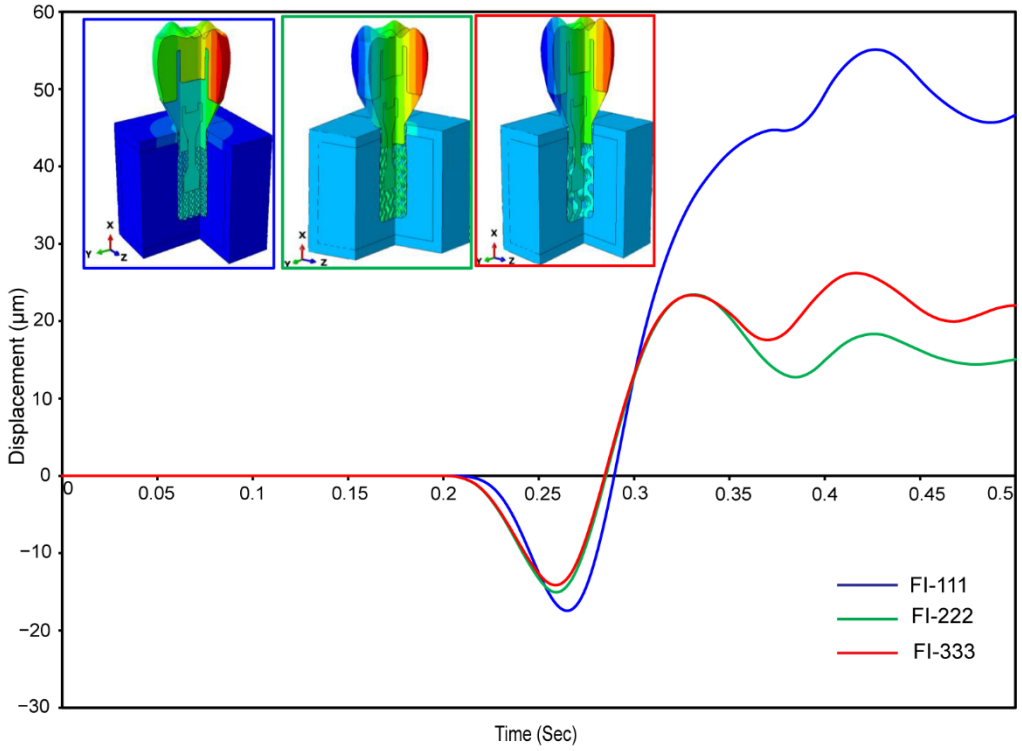

Figure 14. Displacement with in single cycle of mastication for fully latticed configuration at various cell size (FI-111, FI-222, and FI-333).

As the cycle progresses, the displacement exhibits dynamic, cyclic behavior that is consistent with the loading patterns observed during clinical mastication. Specifically, FI-111 shows a large displacement, peaking at 57 micrometers. This implies that it is more flexible under stress, which could affect the micromotion at the bone-implant interface. In comparison, FI-333 and FI-222 have more controlled displacements of 24 micrometers and 17 micrometers, respectively. These changes show the effect of cell size on implant biomechanical performance, with smaller cell sizes (FI-111) allowing for higher displacement and maybe more micromotion, which may compromise osseointegration and stability. The bigger cell sizes (FI-333 and FI-222) exhibit reduced displacement, suggesting a more stable interface under similar loading conditions.

These findings emphasize the importance of lattice structure and cell size in regulating dental implant displacement and subsequent micromotion. Such micromotions are critical for determining the mechanical integration of the implant into the surrounding bone structure, which influences both immediate postoperative stability and long-term osseointegration success.

In Figure 15, you can see in great detail how the displacement responses change for hybrid latticed dental implants with different cell sizes during a single cycle of 0.5 seconds of mastication oblique loading. Initially, all configurations exhibit zero displacement, indicating early stability. However, immediately after 0.215 seconds, displacement shifts negative, dropping to -17 micrometers for HI-333, -14 micrometers for HI-222, and -11.5 micrometers for HI-111 at exactly 0.25

 doi:10.20944/preprints202409.0694.v1

seconds. This implies an initial inward movement under strain, similar to the compressive action seen in masticatory activity.

The displacement then enters a dynamic phase with cyclic fluctuations, including peaks and troughs. At around 0.315 seconds, HI-111 has the most significant peak at 15 micrometers, followed by HI-333 at 0.2875 seconds, and HI-222 at 0.28 seconds. The displacement follows a cyclic pattern with decreasing amplitude, demonstrating the implant structure's durability under cyclic stresses. This cyclic action resembles the normal masticatory process, which is important for determining the implants' biomechanical compatibility and functional stability.

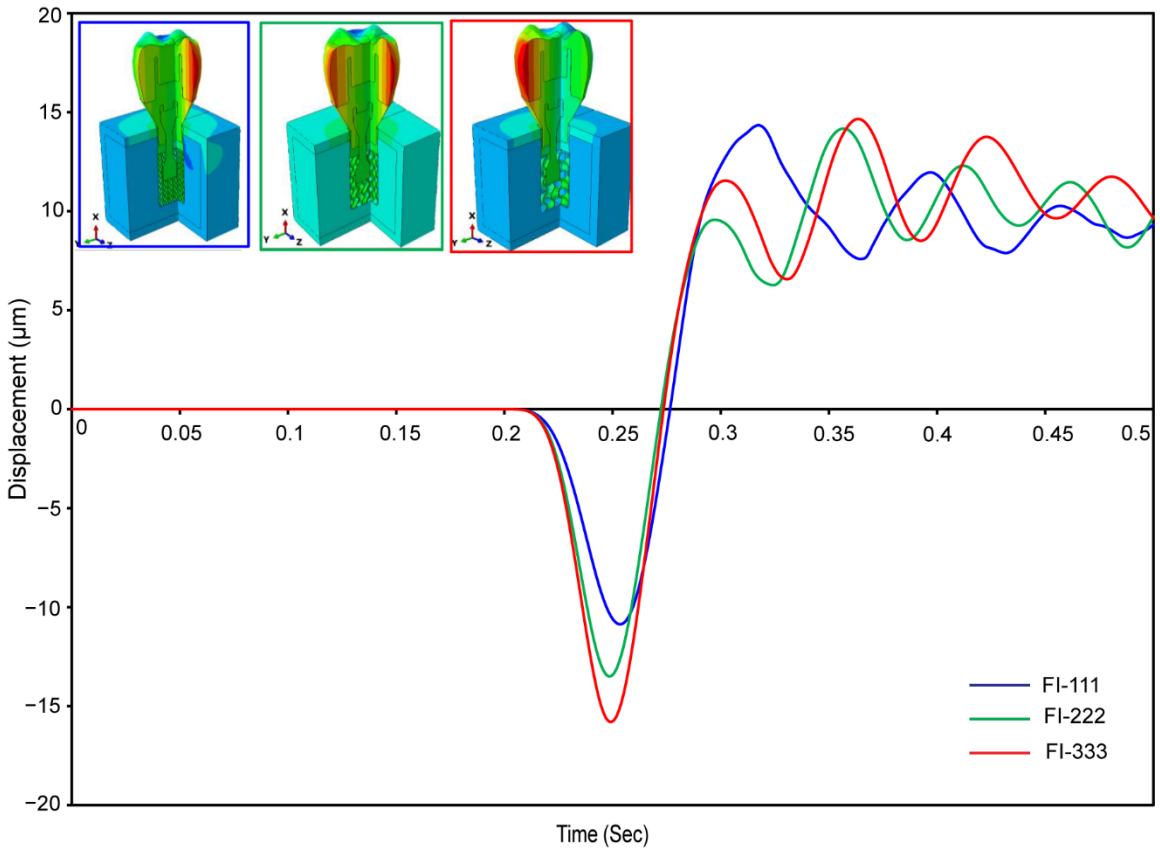

Figure 15. Displacement with in single cycle of mastication for hybrid latticed configuration at various cell size (HI-111, HI-222, and HI-333).

Comparing these findings to those from Figure 14 for fully latticed implants, it is noticeable that hybrid latticed implants have lower peak displacements, demonstrating that hybrid arrangements may better limit micromotions at the bone-implant interface. Smaller micromotions promote osseointegration by lowering possible micromechanical instabilities that might jeopardize implant life and success. This nuanced displacement behavior in hybrid implants, characterized by lower peak values and more regulated cyclic changes, highlights their potential for improved clinical performance, especially under dynamic loading circumstances similar to normal masticatory activities.

4. Discussion

The results of our dynamic explicit finite element analyses provide compelling evidence supporting the hypothesis outlined in the introduction: the hybrid latticed dental implant configuration outperforms the fully latticed design across all three cell sizes considered. This enhanced performance is most noticeable in the management of micromotions under cyclic masticatory loading and the optimization of mechanical characteristics. These are critical for dental implants' longevity and effectiveness. Figure 5 shows a thorough simulation that demonstrates a

 doi:10.20944/preprints202409.0694.v1

major breakthrough in our knowledge of dental implant activity under realistic masticatory settings. By putting an oblique dynamic load of 118.2 N on the occlusal surface of the dental crown and recording detailed stress patterns over a 0.5-second period of time, this study successfully simulated a 2 Hz mastication cycle. The small changes in load along the mesiodistal, buccal-lingual, and apical orientations, made possible by the smart use of multi-point constraints (MPC), show how well and precisely the simulations of real-life chewing forces can be controlled. The accuracy of this work's methods makes stress simulations in fully and hybrid latticed dental implants more reliable. This connects theoretical models to clinical results successfully. It validates the implants' biomechanical integrity by ensuring that the load distribution closely conforms to prescribed specifications. This demonstrates the simulation tools' ability to reliably predict clinical performance and validates their effectiveness. This alignment emphasizes the importance of dynamic loading models in the preclinical evaluation of dental implants, providing the groundwork for future breakthroughs in implant design and testing.

Figure 6 shows that among fully latticed dental implants, the FI-333 design, with a largest cell size of 3x3x3, has the lowest von Mises stress at 388.05 MPa, indicating excellent stress distribution and mechanical stability. This trend shows that bigger cell sizes in fully latticed implants improve stress distribution, lowering overall stress levels inside the implant structure. In contrast, Figure 7 depicts a more complicated pattern in hybrid latticed implants, with the medium-sized HI-222 experiencing the maximum stress at 420.53 MPa, as opposed to its smaller and larger counterparts. This non-linear stress distribution in hybrid designs implies that, although increasing cell size typically increases stress dispersion, there may be an optimal cell size that adequately balances mechanical characteristics and stiffness. The results show an important idea: for hybrid latticed implants, the best cell size seems to be either smaller or bigger than the medium size, based on their mechanical properties. This is because HI-111 and HI-333 both have lower stress levels than HI-222. This distinction between fully latticed and hybrid latticed designs emphasizes the intricate relationship between lattice architecture and stress management in dental implants. It suggests that while complete latticed structures typically favor larger cell sizes for enhanced mechanical performance, hybrid designs may require meticulous cell size adjustments to achieve the best biomechanical outcomes.

Figure 8 and Figure 9 shows a striking comparison of maximum von Mises stresses in fully and hybrid gyroid latticed dental implants and their accompanying retention screws at various cell sizes. In fully latticed implants, stress reduces consistently with increasing cell size: the smallest FI-111 implant has the maximum stress at 410.1 MPa, which reduces to 322.1 MPa for FI-222 and 300.95 MPa for FI-333 (refer to Figure 8a). This pattern indicates that higher cell sizes improve stress distribution, possibly increasing the implant's mechanical stability and function. Similarly, the accompanying retention screws follow a similar pattern, with stress decreasing from 450.31 MPa in the FI-111 to 320.31 MPa in the FI-333, demonstrating how cell size optimization may improve overall implant system integrity (refer to Figure 9a).

In contrast, hybrid latticed implants show a more varied stress distribution(refer to Figure 8 and Figure 9). The HI-111 model shows a stress of 344.06 MPa, which is lower than its completely latticed counterpart but still significant. HI-222 and HI-333 have stresses of 339.89 MPa and 280.39 MPa, respectively (refer to Figure 8b). This means that as cell size increases, the stress decreases less predictably than in fully latticed models. The stress of hybrid model retaining screws varies greatly, with the HI-111 screw having a much lower stress of 133.03 MPa (refer to Figure 9b). This implies that hybrid structures may handle stress differently, perhaps providing better structural details that affect load distribution. The use of a solid neck in hybrid lattice structures improves the structural stability of dental implants, which is especially useful in high porosity designs, such as completely latticed models. This characteristic redistributes stress, lowering concentrations that might cause damage, particularly in areas like the implant neck and initial thread. The hybrid lattice architecture, as shown by the HI-111 model with its reduced cell size, has improved stress distribution and mechanical characteristics. This arrangement not only enhances the implant's functional lifetime by preventing mechanical failures, but it also protects accompanying components such as retaining

 doi:10.20944/preprints202409.0694.v1

screws and surrounding bones. Hybrid latticed implants find the best balance between porosity and strength by increasing cell size and adding solid structural elements. This leads to new implant designs that meet both biomechanical and clinical standards.

The biomechanical implications of the stress distribution patterns shown in Figure 10 and 11 give fundamental insights into the design effectiveness of completely and hybrid latticed dental implants from a dentistry, biomechanical, and materials science viewpoint. The FI-333 configuration exhibits the highest stress concentration in cortical bone among fully latticed designs (refer to Figure 10a), which is an important result since this area has a direct impact on the implant's stability and lifetime. High stress concentrations at the implant-bone contact, especially around the neck, as seen in FI-333, may predispose the implant to mechanical failures caused by increased strain during mastication, underscoring the need for carefully considering implant shape in load-bearing locations.

In contrast, the FI-222 model, which has much lower stress levels in both bone types(refer to Figure 10a and 10b), shows an ideal cell size that allows for better stress distribution, possibly increasing implant longevity and lowering biomechanical problems such as bone resorption. This shows that mid-range cell sizes in completely latticed implants may provide a mix of structural integrity and flexibility, resulting in more efficient stress absorption and redistribution.

In the case of hybrid latticed implants, as shown in Figure 11, the HI-333 model exhibits a high peak stress inside cancellous bone (refer to Figure 11b) , suggesting possible weaknesses in regions of intimate contact between the implant and bone. This significant stress concentration emphasizes the vital necessity for accurate designing of lattice structures to reduce localized stress peaks that might jeopardize implant performance. On the other hand, the HI-222 has much lower stress levels ((refer to Figure 11a and 11b)), making it the ideal cell size for hybrid designs. This construction not only reduces stress in critical locations, but it also exhibits the efficacy of combining a solid neck with a latticed body to improve overall stress distribution. The HI-222's improved efficacy in controlling biomechanical stresses shows a synergistic impact of lattice design and cell size, which properly balance stiffness and flexibility to bear physiological loads while preserving the bone-implant contact.

The hybrid design of dental implants, especially those with a solid neck, considerably improves stress distribution in both cortical and cancellous bones, which is critical for implant integration and lifespan. This design method efficiently reduces mechanical stresses throughout the implant, particularly in stress-prone locations near the implant-bone contact. This characteristic effectively reduces peak stress concentrations commonly found around the holes of cortical and cancellous bones, aligning with prior research that pinpoints potential sites for bone resorption. The hybrid design with a solid neck reduces localized stress peaks that may contribute to bone damage by distributing stresses more uniformly, improving the implant's stability and functional longevity. Among the hybrid models studied, the HI-222 design performs best by combining lattice flexibility with the durability of a solid structure, making it perfect for addressing both problems of mechanical load control and bone preservation. This configuration not only provides a biomechanically favorable environment, but it also significantly reduces the likelihood of implant failure, making it an excellent choice for patients who are prone to bone resorption, better aligning dental implant designs with both mechanical demands and biological compatibilities.

Figure 12 and 13 offer a comparative investigation of key biomechanical characteristics of fully hybrid latticed dental implants, with an emphasis on the variation in stress distribution throughout the crown and abutment components. In Figure 12, the crown components of completely latticed implants show modest stress levels, which contrast strikingly with the much greater strains detected in the abutment components. This significant discrepancy, particularly with FI-222 reaching an unusually high stress of 777.65 MPa, highlights the possibility of localized overstressing, which might impair mechanical integrity under typical clinical loads.

Figure 13 shows that hybrid latticed implants not only have higher stress levels in the crown than completely latticed implants, but they also have much lower and more balanced stresses in the abutment portions. This pattern shows that hybrid designs, most likely combining several lattice topologies with a solid neck, improve stress dissipation. Such structural advances considerably

 doi:10.20944/preprints202409.0694.v1

increase implant lifetime and performance by lowering the possibility of stress concentrations, which often cause implant failure. Notably, HI-222's stress profile, with the lowest abutment stress of 17.31 MPa, demonstrates its biomechanical effectiveness and structural resilience.

These findings highlight the significance of lattice cell size and layout in designing dental implant designs to achieve a balance of mechanical stability and effective stress distribution. Specifically, hybrid latticed designs, notably the HI-222 form illustrated in Figure 13, provide an ideal cell size that offers a strategic balance of stiffness and flexibility. This arrangement is appropriate for clinical circumstances in which consistent stress distribution is critical to the implant's effectiveness. Figures 12 and 13 show important new findings that will help advance dental implant technology. They show a shift in strategy toward designs that may better control biomechanical stresses while improving clinical outcomes.

Figure 14 and 15 show the dynamic displacement responses of fully hybrid latticed dental implants throughout a mastication cycle, which give a thorough knowledge of the biomechanical behavior and clinical consequences of various lattice configurations. Figure 14 demonstrates that cell size directly determines the varying displacement and micromotion of fully latticed implants. The highest displacements recorded in FI-111, peaking at 57 micrometers, indicate a greater degree of flexibility under load, which may increase micromotion at the bone-implant interface. Such increased micromotion may impair osseointegration and stability, especially in clinical situations when bone integrity is critical. FI-333 and FI-222, on the other hand, have bigger and medium cell sizes and more controlled displacements of 24 and 17 micrometers, respectively. This suggests a more stable interface, which will probably improve mechanical integration and lower the chance of implant failure.

Figure 15 shows how hybrid latticed implants have substantially diverse displacement patterns. Notably, these implants exhibit smaller peak displacements, which may indicate more effective micromotion regulation. For example, HI-111 peaks at just 15 micrometers, which is substantially lower than its fully latticed equivalent, implying that the hybrid design's combination of lattice and solid structures may be more effective at stress distribution and micromotion minimization. This feature is critical for improving osseointegration because excessive micromotion could disrupt the intricate equilibrium required for bone formation and implant integration.

These findings highlight the substantial role of lattice structure and cell size in affecting the mechanical properties of dental implants. According to the results, hybrid latticed designs, especially those with smaller and bigger cell sizes like HI-111 and HI-333, give a biomechanical advantage by minimizing micromotions and perhaps enhancing clinical outcomes for dental implants. The decreased stress and displacement levels in hybrid designs lead to an optimal cell size and arrangement that better meets the mechanical demands of the masticatory environment, indicating a potential route for future implant designs aiming to enhance clinical effectiveness and lifespan.

5. Conclusions

This research investigates the biomechanical performance of dental implants, with an emphasis on the effects of lattice structure and cell size on stress distribution, mechanical stiffness, and micromotion stability. The study's goal is to improve clinical outcomes by comparing fully gyroid latticed and hybrid gyroid latticed implants with a solid neck across various cell sizes. The investigation came to the following key conclusions:

- Hybrid latticed implants, especially those with medium cell sizes (HI-222), exhibit excellent stress distribution. These designs efficiently lower stress concentrations in crucial locations, possibly improving implant lifetime and success.
- In comparison to fully latticed implants, hybrid designs provide higher mechanical rigidity. This improvement is critical for preserving structural integrity under typical masticatory stresses, which is necessary for the implants' long-term durability.
- The researchers discovered that hybrid latticed implants with solid necks had significantly reduced micromotions at the bone-implant contact. This decrease is critical for improving

 doi:10.20944/preprints202409.0694.v1

osseointegration and lowering the possibility of implant failure due to biomechanical instabilities.

- Tailored hybrid latticed designs with optimal cell sizes show promise in clinical applications, outperforming standard fully latticed implants. The HI-222 arrangement is especially advantageous, offering a mix of flexibility and load-bearing capability appropriate for a wide range of clinical conditions.
- Adding a solid neck to hybrid latticed implants makes stress distribution much better, managing stress in a way that a fully latticed configuration can't. Medium-sized cells, particularly in hybrid topologies like HI-222, function optimally, establishing new standards in dental implant design by combining light weight with high mechanical characteristics.
- This research demonstrates the efficacy of additive manufacturing for producing biomechanically optimized dental implants. These improved manufacturing procedures substantially enhance patient outcomes by precisely matching bone's inherent biomechanical characteristics, indicating an optimistic future for dental implant technology.

These findings emphasize the need for rigorous design and material selection in the creation of dental implants in order to fulfill the stringent demands of clinical application. The study's results provide a basis for future research and development in dental implant technologies, with the goal of achieving optimum biomechanical compatibility and performance.

Author Contributions: Conceptualization, D.B.A, M.T, and S.J-H.; methodology, D.B.A, S.J-H, and M.T.; software, D.B.A, M.T, and S.J-H.; validation, D.B.A,S.J-H. and M.T.; formal analysis, D.B.A.; investigation, D.B.A.; data curation, D.B.A,; writing—original draft preparation, D.B.A ; writing—review and editing, D.B.A., M.T., S.J-H.; supervision, M.T. and S.J.H; project administration, S.J-H and M.T. All authors have read and agreed to the published version of the manuscript.

Funding: This research was funded by the National Science and Technology Council (Taiwan) (project No. 111-2221-E-011 -096 -MY3) and partially supported by MEXT Grant-in-Aid for Scientific Research (A) (Grant No. 21H04731).

Data Availability Statement: The original contributions presented in the study are included in the article, further inquiries can be directed to the corresponding author.

Acknowledgments: The authors would like to acknowledge the financial support from the National Science and Technology Council (Taiwan) and MEXT Grant-in-Aid for Scientific Research (A). The authors also express their thanks for using QuillBot's AI-powered paraphrase tool, which offers spelling, grammar, and plagiarism checking services at **https://quillbot.com/** (accessed on 28 February 2024).

Conflicts of Interest: The authors declare no conflict of interest.

References

1. Yan, G.; Sun, M.; Zhang, Z.; Liang, Y.; Jiang, N.; Pang, X.; Song, Y.; Liu, Y.; Zhao, J. Experimental Study on Flow and Heat Transfer Performance of Triply Periodic Minimal Surface Structures and Their Hybrid Form as Disturbance Structure. *Int. Commun. Heat Mass Transf.* **2023**, *147*, 106942.
2. Hussain, M.I.; Xia, M.; Ren, X.; Ge, C.; Jamil, M.; Gupta, M.K. Digital Light Processing 3D Printing of Ceramic Materials: A Review on Basic Concept, Challenges, and Applications. *Int. J. Adv. Manuf. Technol.* **2024**, *130*, 2241–2267.
3. Fu, H.; Kaewunruen, S. The Axially-Loaded Behaviours of Schwarz Primitive (SP)-Based Structures: An Experimental and DEM Study. *Thin-Walled Struct.* **2024**, *200*, 111973.
4. Anju, S.; Prajitha, N.; Sukanya, V.S.; Mohanan, P. V Materials Today Chemistry. *Mater. Today* **2020**, *16*, 100236.
5. Sundaramoorthy, R.; Raja Balayanan, S.R. Additive Manufacturing of Composites for Biomedical Implants. *High-Performance Compos. Struct. Addit. Manuf. Process.* **2022**, 125–154.
6. Wanniarachchi, C.T.; Arjunan, A.; Baroutaji, A.; Singh, M.; Robinson, J.; Vance, A.; Appiah, M.; Arafat, A. 3D Printed CoCrMo Personalised Load-Bearing Meta-Scaffold for Critical Size Tibial Reconstruction. *Ann. 3D Print. Med.* **2024**, *15*, 100163.
7. Zhu, Y.; Tang, T.; Zhao, S.; Joralmon, D.; Poit, Z.; Ahire, B.; Keshav, S.; Raje, A.R.; Blair, J.; Zhang, Z. Recent Advancements and Applications in 3D Printing of Functional Optics. *Addit. Manuf.* **2022**, *52*, 102682.
8. Yang, Y.; Jiang, R.; Han, C.; Chen, J.; Li, H.; Wang, Y.; Tang, J.; Zhou, H.; Hu, W.; Zheng, B. Frontiers in Laser Additive Manufacturing Technology. *Addit. Manuf. Front.* **2024**, 200160.

9. Lai, K.-C.; Tsai, C.; Yen, S.-Y.; Tseng, K.-K.; Yeh, J.-W.; Chen, P.-Y. Fabrication of Novel 316L Stainless Steel Scaffolds by Combining Freeze-Casting and 3D-Printed Gyroid Templating Techniques. *Mater. Sci. Eng. A* **2024**, 147200.
10. Araya, M.; Jaskari, M.; Rautio, T.; Guillén, T.; Järvenpää, A. Assessing the Compressive and Tensile Properties of TPMS-Gyroid and Stochastic Ti64 Lattice Structures: A Study on Laser Powder Bed Fusion Manufacturing for Biomedical Implants. *J. Sci. Adv. Mater. Devices* **2024**, *9*, 100663.
11. Rezapourian, M.; Kumar, R.; Hussainova, I. Effect of Unit Cell Rotation on Mechanical Performance of Selective Laser Melted Gyroid Structures for Bone Tissue Engineering. *Prog. Eng. Sci.* **2024**, *1*, 100011.
12. Sheng, X.; Liu, H.; Xu, Y.; Wang, Z.; Zhang, W.; Li, C.; Wang, J. Functionalized Biomimetic Mineralized Collagen Promotes Osseointegration of 3D-Printed Titanium Alloy Microporous Interface. *Mater. Today Bio* **2024**, *24*, 100896.
13. Sheng, X.; Che, Z.; Qiao, H.; Qiu, C.; Wu, J.; Li, C.; Tan, C.; Li, J.; Wang, G.; Liu, W. A Functional Mineralized Collagen Hydrogel to Promote Angiogenic and Osteogenic for Osseointegration of 3D-Printed Titanium Alloy Microporous Scaffolds. *Int. J. Biol. Macromol.* **2024**, 133806.
14. Abd-Elaziem, W.; Mohammed, M.M.; Yehia, H.M.; Sebaey, T.A.; Khan, T. Porous Titanium for Medical Implants. *Sci. Park Publ* **2024**, *1*, 10–62184.
15. Davidopoulou, S.; Batas, L.; Karakostas, P.; Tortopidis, D.; Barmpalexis, P.; Assimopoulou, A.; Angelopoulos, C.; Tsalikis, L. Multidimensional 3D-Printed Scaffolds for Ridge Preservation and Dental Implant Placement: A Systematic Review. *Appl. Sci.* **2024**, *14*, 892.
16. Zhang, T.; Zhou, W.; Yang, W.; Bi, J.; Li, H.; Gao, X.; Zhang, B.; Shi, G.; Li, K.; Wei, Z. Vancomycin-Encapsulated Hydrogel Loaded Microarc-Oxidized 3D-Printed Porous Ti6Al4V Implant for Infected Bone Defects: Reconstruction, Anti-Infection, and Osseointegration. *Bioact. Mater.* **2024**, *42*, 18–31.
17. Ma, C.; de Barros, N.R.; Zheng, T.; Gomez, A.; Doyle, M.; Zhu, J.; Nanda, H.S.; Li, X.; Khademhosseini, A.; Li, B. 3D Printing and Surface Engineering of Ti6Al4V Scaffolds for Enhanced Osseointegration in an In Vitro Study. *Biomimetics* **2024**, *9*, 423.
18. Miao, X.; Hu, J.; Xu, Y.; Su, J.; Jing, Y. Review on Mechanical Properties of Metal Lattice Structures. *Compos. Struct.* **2024**, 118267.
19. Dalave, P.A.; Joseph, T.; Patil, D.; Patadiya, J.; Naebe, M.; Kandasubramanian, B. Meta-Structures for Energy Absorption: Materials, Designs, and Applications in Additive Manufacturing and Its Future Scope. *J. Brazilian Soc. Mech. Sci. Eng.* **2024**, *46*, 518.
20. He, S.; Zhu, J.; Jing, Y.; Long, S.; Tang, L.; Cheng, L.; Shi, Z. Effect of 3D-Printed Porous Titanium Alloy Pore Structure on Bone Regeneration: A Review. *Coatings* **2024**, *14*, 253.
21. Shahid, M.N.; Shahid, M.U.; Rasheed, S.; Irfan, M.; Obeidi, M.A. Computational Investigation of the Fluidic Properties of Triply Periodic Minimal Surface (TPMS) Structures in Tissue Engineering. *Designs* **2024**, *8*, 69.
22. Maevskaia, E.; Ghayor, C.; Bhattacharya, I.; Guerrero, J.; Weber, F.E. TPMS Microarchitectures for Vertical Bone Augmentation and Osteoconduction: An In Vivo Study. *Materials (Basel).* **2024**, *17*, 2533.
23. Peng, X.; Li, S.; He, D.; Li, J.; Qu, S.; Jin, Z. Expanding the Mechanical and Mass-Transport Combination for Bone Scaffolds: Through Stretched Structure. *Compos. Struct.* **2024**, *329*, 117783.
24. Taheri, A.; Farahmand, F.; Bahraminasab, M. Radially and Axially Graded Cellular Tibial Stems for Total Knee Replacement. *Int. J. Mech. Sci.* **2024**, *263*, 108772.
25. Wakjira, Y.; Cioni, A.; Lemu, H.G. Current Status of the Application of Additive-Manufactured TPMS Structure in Bone Tissue Engineering. *Prog. Addit. Manuf.* **2024**, 1–18.
26. Joshua, R.J.N.; Raj, S.A.; Hameed Sultan, M.T.; Łukaszewicz, A.; Józwik, J.; Oksiuta, Z.; Dziedzic, K.; Tofil, A.; Shahar, F.S. Powder Bed Fusion 3D Printing in Precision Manufacturing for Biomedical Applications: A Comprehensive Review. *Materials (Basel).* **2024**, *17*, 769.
27. Gao, J.; Pan, Y.; Gao, Y.; Pang, H.; Sun, H.; Cheng, L.; Liu, J. Research Progress on the Preparation Process and Material Structure of 3D-Printed Dental Implants and Their Clinical Applications. *Coatings* **2024**, *14*, 781.
28. Huang, X.; Lou, Y.; Duan, Y.; Liu, H.; Tian, J.; Shen, Y.; Wei, X. Biomaterial Scaffolds in Maxillofacial Bone Tissue Engineering: A Review of Recent Advances. *Bioact. Mater.* **2024**, *33*, 129–156.
29. Chen, H.; Song, G.; Xu, T.; Meng, C.; Zhang, Y.; Xin, T.; Yu, T.; Lin, Y.; Han, B. Biomaterial Scaffolds for Periodontal Tissue Engineering. *J. Funct. Biomater.* **2024**, *15*, 233.
30. Поведение, К.; Чистого, Alemayehu, D.B, Т.; Различной, Т.С. CORROSION BEHAVIOR OF COMMERCIALLY-PURE TITAMIUM WITH DIFFERENT MICROSTRUCTURES. **2017**, *171*, 167–171.
31. Исследования, Т.; Технически, Alemayehu, D.B, Н.А.; Титане, Ч.; Микроструктурой, Р.; Без, С.П.И. TRIBOLOGICAL STUDIES FOR COMMERCIALLY PURE GRADE 4 TITANIUM WITH DIFFERENT MICROSTRUCTURES , WITH AND WITHOUT COATING. **2018**, *6*, 3–6.
32. Semenov, V.I.; Alemayehu, D.B.; Schuster, L.S.; Raab, G.I.; Chertovskikh, S. V.; Astanin, V. V.; Huang, S.J.; Chernyak, I.N. Tribotechnical Characteristics of Commercially Pure Titanium with Different Grain Sizes and TiC and TiO2 Coatings. *J. Frict. Wear* **2019**, *40*, 349–354, doi:10.3103/S1068366619040111.

33. Semenov, V.I.; Valiev, R.R.; Belov, P.A.; Bogale, D. FEATURES OF CORROSION BEHAVIOR OF COMMERCIALLY-PURE TITAMIUM WITH DIFFERENT MICROSTRUCTURES.
34. Alemayehu, D.B.; Todoh, M.; Hsieh, J.-H.; Li, C.; Huang, S.-J. Improving Pure Titanium's Biological and Mechanical Characteristics through ECAP and Micro-Arc Oxidation Processes. *Micromachines* 2023, *14*.
35. Zhang, C.; Qiao, H.; Yang, L.; Ouyang, W.; He, T.; Liu, B.; Chen, X.; Wang, N.; Yan, C. Vibration Characteristics of Additive Manufactured IWP-Type TPMS Lattice Structures. *Compos. Struct.* **2024**, *327*, 117642.
36. Xu, P.; Guo, W.; Yang, L.; Yang, C.; Ruan, D.; Xu, J.; Yao, S. Crashworthiness Analysis of the Biomimetic Lotus Root Lattice Structure. *Int. J. Mech. Sci.* **2024**, *263*, 108774.
37. Luo, J.; Peng, S.; Hou, S.; Kiani, Y. Vibration Analysis of FGM Anisogrid Lattice Plates with One Width Fold Based on the Continuous Model Using the GDQE Method. *Thin-Walled Struct.* **2024**, *195*, 111386.
38. Bruggeman, K.; Palazotto, A.N. Characterization of Triply Periodic Minimal Structures for Additive Manufacturing Production and Residual Stress Analysis. In Proceedings of the AIAA SCITECH 2024 Forum; 2024; p. 2076.
39. Eremin, A. V; Frolov, M.A.; Krutov, A.F.; Smolkov, M.I.; Shulga, A.S.; Bragin, D.M.; Popov, A.I.; Blatov, V.A. Mechanical Properties of Porous Materials Based on New Triply Periodic and Minimal Surfaces. *Mech. Adv. Mater. Struct.* **2024**, 1–17.
40. Tkac, J.; Toth, T.; Mizera, O.; Molnar, V.; Fedorko, G.; Dovica, M. Comparison of Quality of Porous Structure Specimens Produced by Different Additive Technologies and from Different Materials. *Appl. Sci.* **2024**, *14*, 648.
41. Wang, L.; He, L.; Liu, F.; Yuan, H.; Li, J.; Chen, M. Mechanical Characterization of Multifunctional Metal-Coated Polymer Lattice Structures. *Materials (Basel).* **2024**, *17*, 741.
42. Monteiro, B.; Rocha, F.; Costa, J. Topology Optimization of a Robot Gripper with NTopology. *U. Porto J. Eng.* **2024**, *10*, 11–19.
43. Munyensanga, P.; Bricha, M.; El Mabrouk, K. Functional Characterization of Biomechanical Loading and Biocorrosion Resistance Properties of Novel Additively Manufactured Porous CoCrMo Implant: Comparative Analysis with Gyroid and Rhombic Dodecahedron. *Mater. Chem. Phys.* **2024**, *316*, 129139.
44. Bhat, C.; Prajapati, M.J.; Kumar, A.; Jeng, J.-Y. Additive Manufacturing-Enabled Advanced Design and Process Strategies for Multi-Functional Lattice Structures. *Materials (Basel).* **2024**, *17*, 3398.
45. Moya, B.J.; Rivas, M.; Quiza, R.; Davim, J.P. Computer Simulation-Based Multi-Objective Optimisation of Additively Manufactured Cranial Implants. *Technologies* **2024**, *12*, 125.
46. Chibinyani, M.I.; Dzogbewu, T.C.; Maringa, M.; Muiruri, A. Lattice Structures Built with Different Polygon Hollow Shapes: A Review on Their Analytical Modelling and Engineering Applications. *Appl. Sci.* **2024**, *14*, 1582.
47. Alemayehu, D.B.; Todoh, M.; Huang, S.-J. Advancing 3D Dental Implant Finite Element Analysis: Incorporating Biomimetic Trabecular Bone with Varied Pore Sizes in Voronoi Lattices. *J. Funct. Biomater.* **2024**, *15*, 94.
48. Rayhan, M.T.; Rimon, M.I.H.; Khan, M.; Hasan, M.A.; Mobarak, M.H.; Islam, M.A.; Hossain, N. Advances in Additive Manufacturing of Nanocomposite Materials Fabrications and Applications. *Eur. Polym. J.* **2024**, 113406.
49. Nazir, A.; Waqar, S.; ul Haq, M.R.; Tanveer, M.Q. Design for Additive Manufacturing of Cellular Structures. In *Additive Manufacturing Materials and Technology*; Elsevier, 2024; pp. 359–388.
50. Alkunte, S.; Fidan, I.; Naikwadi, V.; Gudavasov, S.; Ali, M.A.; Mahmudov, M.; Hasanov, S.; Cheepu, M. Advancements and Challenges in Additively Manufactured Functionally Graded Materials: A Comprehensive Review. *J. Manuf. Mater. Process.* **2024**, *8*, 23.
51. Mrówczyński, D.; Gajewski, T.; Pośpiech, M.; Garbowski, T. Estimation of the Compressive Strength of Cardboard Boxes Including Packaging Overhanging on the Pallet. *Appl. Sci.* **2024**, *14*, 819.
52. Alemayehu, D.-B.; Jeng, Y.-R. Three-Dimensional Finite Element Investigation into Effects of Implant Thread Design and Loading Rate on Stress Distribution in Dental Implants and Anisotropic Bone. *Materials (Basel).* 2021, *14*.
53. Alemayehu, D.B.; Todoh, M.; Huang, S. Nonlinear Finite Element Analysis of Bone-Implant Contact in Three Short Dental Implant Models with Varying Osseointegration Percentages Nonlinear Finite Element Analysis of Bone-Implant Contact in Three Short Dental Implant Models with Varying Osseointegration Percentages. **2024**, doi:10.20944/preprints202408.2180.v1.
54. Alemayehu, D.B.; Todoh, M.; Huang, S.J. Advancing 3D Dental Implant Finite Element Analysis: Incorporating Biomimetic Trabecular Bone with Varied Pore Sizes in Voronoi Lattices. *J. Funct. Biomater.* **2024**, *15*, doi:10.3390/jfb15040094.
55. Alemayehu, D.B. Design and Development of Shell and Tube Heat Exchanger for Harar Brewery Company Pasteurizer Application (Mechanical and Thermal Design). *Am. J. Eng. Res.* **2013**, *2*, 99–109.

56. Alemayehu, D.B.; Todoh, M. Enhanced Energy Absorption with Bioinspired Composite Triply Periodic Minimal Surface Gyroid Lattices Fabricated via Fused Filament Fabrication (FFF). *J. Manuf. Mater. Process.* 2024, *8*.
57. Alemayehu, D.B.; Huang, S.-J.; Koricho, E.G. Experimental and FEM Analysis of Three Carbon Steel Characterization under Quasi-Static Strain Rate for Bumper Beam Application. In Proceedings of the MATEC Web of Conferences; 2017; Vol. 123.
58. Lotavath, J.R.; Bansal, M.; Mds, R.S.; Khan, S.M.; Gajdhar, S.K. Assessment Of Dental Implant Survival Rates Post Platelet-Rich Plasma Treatment : A Comprehensive Analysis. *2706*, 1342–1347.
59. Thakur, S.; Chauhan, S.R. Development of a Critical Edge-Based Adaptive Toolpath Strategy to Improve Geometrical Accuracy of Incrementally Formed Titanium Implants. *J. Manuf. Process.* **2024**, *110*, 114–125, doi:10.1016/j.jmapro.2023.12.053.
60. Meier, T.; Li, R.; Mavrikos, S.; Blankenship, B.; Vangelatos, Z.; Yildizdag, M.E.; Grigoropoulos, C.P. Obtaining Auxetic and Isotropic Metamaterials in Counterintuitive Design Spaces: An Automated Optimization Approach and Experimental Characterization. *npj Comput. Mater.* **2024**, *10*, 3.
61. YÜKSEL, N.; Oğulcan, E.; BÖRKLÜ, H.R.; SEZER, H.K. Mechanical Properties of Additively Manufactured Lattice Structures Designed by Deep Learning. *Thin-Walled Struct.* **2024**, *196*, 111475.
62. Liu, F.; Chen, M.; Liu, S.; Xiang, Z.; Huang, S.; Lim, E.G.; Zhang, S. Stress-Driven Generative Design and Numerical Assessment of Customized Additive Manufactured Lattice Structures. *Mater. Des.* **2024**, *241*, 112956.
63. Hedayati, R.; Alavi, M.; Sadighi, M. Effect of Degradation of Polylactic Acid (PLA) on Dynamic Mechanical Response of 3D Printed Lattice Structures. *Materials (Basel).* **2024**, *17*, 3674.